ADVANCED ENERGY MATERIALS
www.advenergymat.de

Iodine-Stabilized Organic Nanoparticle Dispersions for the Fabrication of 10% Efficient Non-Fullerene Solar Cells

*Felix Manger, Karen Fischer, Philipp Marlow, Holger Röhm, Christian Sprau, and Alexander Colsmann**

High-performance organic solar cells are deposited from eco-friendly semiconductor dispersions by applying reversible electrostatic stabilization while omitting the need for stabilizing surfactants. The addition of iodine fosters the oxidation (p-doping) of the light-harvesting polymer, effectively promoting the electrostatic repulsion of the nanoparticles and hence the colloidal stability of the respective dispersions. The oxidation of polymers with iodine is reversible: after thin-film deposition and after thermal evaporation of the iodine, the corresponding polymer:non-fullerene solar cells yield power conversion efficiencies of up to 10.6%.

1. Introduction

Among the emerging photovoltaic technologies, organic bulk-heterojunction solar cells stand out with a projected fully eco-friendly cradle-to-grave lifecycle, using abundant carbon-based commodities while vastly omitting rare elements and toxic compounds. The combination of lowest material demands and thin film fabrication by large-area printing or coating will enable unsurpassed energy payback times, which are crucial for a rapid ramp-up of solar cell production in light of climate change.

Today, molecular engineering is the most often employed strategy to pave the way toward an eco-friendly deposition of organic bulk-heterojunctions from solution. Long alkyl chains attached to the conjugated backbones of organic semiconductors promote their solubility in halogenated organic solvents and reduce their self-aggregation by steric hindrance.[1] Less harmful aromatic solvents often require an enhanced solubility of the organic semiconductors, facilitated, e.g., by even longer alkyl chains or random co-polymerization.[2,3]

F. Manger, K. Fischer, P. Marlow, H. Röhm, C. Sprau, A. Colsmann
Material Research Center for Energy Systems
Karlsruhe Institute of Technology (KIT)
Strasse am Forum 7, 76131 Karlsruhe, Germany
E-mail: alexander.colsmann@kit.edu
F. Manger, K. Fischer, P. Marlow, H. Röhm, A. Colsmann
Light Technology Institute
Karlsruhe Institute of Technology (KIT)
Engesserstrasse 13, 76131 Karlsruhe, Germany

The ORCID identification number(s) for the author(s) of this article can be found under https://doi.org/10.1002/aenm.202202820.

DOI: 10.1002/aenm.202202820

An entirely different route to the eco-friendly processing of organic semiconductor thin films is their deposition from aqueous or alcoholic dispersions,[4] reinforcing the unique environmental sustainability of organic solar cells. Recent reports also featured acetonitrile as a promising dispersion agent due to its high permittivity and hence its excellent screening of stabilizing charges.[5] Besides the omission of toxic solvents during coating, this deposition route i) disentangles solution processing from the need of solubility, ii) advances multi-layer deposition without the need for orthogonal solvents and hence iii) is less dependent on molecular engineering, eventually giving access to a broader choice of semiconductors for optoelectronic applications.[6] The prevailing challenge of this approach is the colloidal stabilization of the dispersion.[7,8] Only very few organic semiconductors exhibit sufficient intrinsic colloidal stability, with its most prominent example being poly(3-hexylthiophene-2,5-diyl) (P3HT). Its high intrinsic colloidal stability allows the synthesis of P3HT nanoparticle dispersions by rapid solvent exchange, where a P3HT solute is nanoprecipitated upon injection into miscible ethanol.[9,10] The high colloidal stability of P3HT also enables the formation of nanoparticle dispersions of blends of P3HT and indene-C_{60} bisadduct (ICBA). Such P3HT:ICBA nanoparticle dispersions can be synthesized with reasonably high concentrations and can be used as inks to fabricate solar cells with maximum power conversion efficiencies (PCEs) of 4.5%.[11]

Other organic semiconductors such as the latest high-performance combinations of polymers and non-fullerene acceptors do not exhibit this intrinsic colloidal stability. To disperse organic semiconductors that would otherwise coagulate rapidly, surfactants have been introduced as stabilizing agents. Best results on the stabilization of organic nanoparticle dispersions were achieved by employing poloxamers, but extensive subsequent purification steps were needed to reduce the final surfactant content which otherwise would have remained in the light-harvesting layer where it would have hampered the solar cell performance.[12,13] Still, this concept produced nanoparticulate solar cells with PCEs of 7.5%.[8]

Recently, we found that the intrinsic colloidal stability of P3HT stems from its unusual but well-known tendency to electrically charge itself which in turn fosters electrostatic repulsion of the nanoparticles.[7] Accordingly, extrinsic oxidation of the light-harvesting polymers, e.g. by electrical p-doping with F_4TCNQ or temporarily even by photodoping with visible light, can enhance the colloidal stability of nanoparticle dispersions.[5,7] Yet, the large ionization potentials of most high-performance light-harvesting polymers render

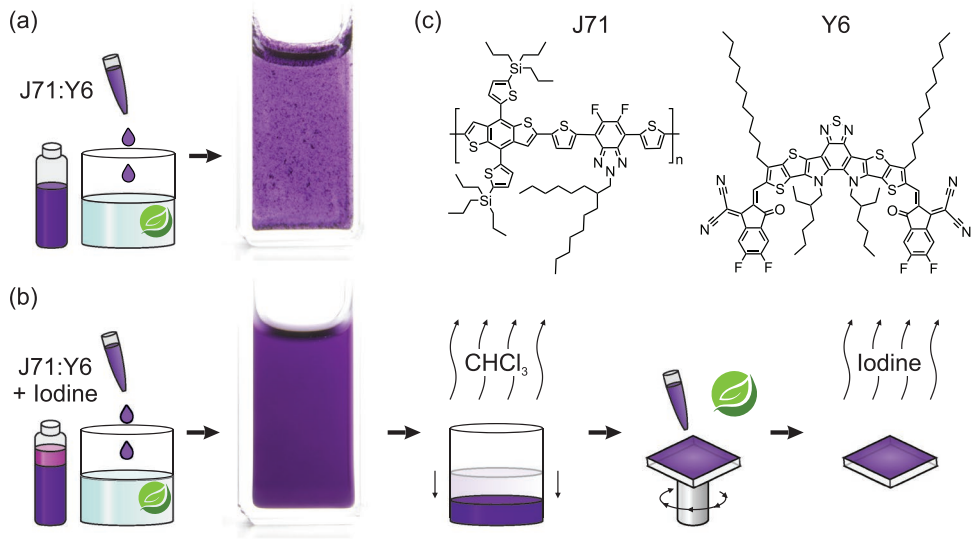

Figure 1. Schematic of the organic nanoparticle synthesis and processing featuring reversible electrostatic stabilization (RES). a) Upon injection of a J71:Y6/chloroform solution into an excess of acetonitrile, the organic semiconductors coagulate, rapidly leading to a visible macroscopic phase separation. b) In contrast, if iodine is added to the J71:Y6 solution prior to injection into acetonitrile, a stable and homogeneous nanoparticle dispersion forms. Afterwards, heating of the dispersion removes the chloroform and increases the concentration of the dispersion. The resulting nanoparticle dispersions are stable and can be used to deposit light-harvesting bulk-heterojunctions, e.g., by spin-coating. During subsequent thermal treatment of the layers at 180 °C, the nanoparticles are joined for best charge carrier transport and the volatile iodine evaporates from the thin films. c) Chemical structures of the polymer donor J71 and the molecular acceptor Y6.

electrical doping often inefficient and would call for substantial amounts of dopants that would later conflict with device operation.[5]

In this work, using highly diffusive and volatile iodine, we introduce the concept of reversible electrostatic stabilization (RES) by oxidation, i.e., a reversible electrical p-doping process, to enhance the colloidal stability of nanoparticle dispersions comprising high-performance polymer donors and non-fullerene acceptors. After thin film deposition from these dispersions, iodine evaporates from the light-harvesting layer, leaving behind a neat bulk-heterojunction which produces solar cells with hero PCEs of 10.6%.

2. Results and Discussion

Figure 1 illustrates the synthesis of the dispersions by nanoprecipitation (i.e., rapid solvent displacement) facilitated by RES. Both the polymer poly[[5,6-difluoro-2-(2-hexyldecyl)-2H-benzotriazole-4,7-diyl]-2,5-thiophenediyl[4,8-bis[5-(tripropylsilyl)-2-thienyl]benzo[1,2-b:4,5-b″]dithiophene-2,6-diyl]-2,5-thiophenediyl] (J71) and the non-fullerene acceptor 2,2″-((2Z,2″Z)-((12,13-bis(2-ethylhexyl)-3,9-diundecyl-12,13-dihydro-[1,2,5]thiadiazolo[3,4-e]thieno[2″,3‴:4′,5″]thieno[2″,3″:4,5]pyrrolo[3,2-g]thieno[2″,3′:4,5]thieno[3,2-b]indole-2,10-diyl)bis(methanylylidene))bis(5,6-difluoro-3-oxo-2,3-dihydro-1H-indene-2,1-diylidene))dimalononitrile (Y6) were dissolved in chloroform (solvent), each at a concentration of 1 g L^{-1}, and then the mixture was injected into acetonitrile (non-solvent). J71 was chosen for its high performance despite its shallow ionization potential E_{IP} = 5.0 eV (measured by photo-electron spectroscopy in air, PESA) which allows p-doping. Acetonitrile was chosen for its high permittivity (ε_r = 36.6), supporting the separation of stabilizing charges and counter-ions.[5,14,15] The miscibility of solvent and non-solvent led to an immediate reduction of solubility and hence to the rapid formation of nanoparticles. In absence of any stabilizing agent, strong and visible coagulation of the dispersion occurred (Figure 1a), rendering the dispersion useless for any further processing. In contrast, upon the addition of iodine to the J71:Y6 solution prior to nanoprecipitation, the resulting J71:Y6 dispersions appeared haze-free, indicating no detrimental coagulation of the dispersion (Figure 1b). The dopant iodine was used before to enhance the conductivity of organic semiconductors, in particular polyacetylene.[16] While the strong volatility of iodine led to its replacement in many optoelectronic thin-film applications that required long-term stable electrical doping, here, we appreciate the very same property to remove the iodine from the light-harvesting layer later. Yet, despite the high volatility of iodine, the J71:Y6 dispersions remained stable for several hours, could be heated to reduce their volume and hence to increase the semiconductor concentration in dispersion.

To gain a fundamental understanding of the underlying processes, we first investigated the electrostatic stabilization of neat J71 dispersions upon the addition of iodine (mass ratio $0 \leq \zeta_{I2/J71} \leq 80$ wt.%, where $\zeta_{I2/J71} = m_{iodine} \cdot m_{J71}^{-1}$), before extending the concept to J71:Y6 blends below. For the synthesis of iodine-stabilized J71 dispersions, suitable amounts of iodine/chloroform solutions (10 g L^{-1}) were added to the J71/chloroform solutions (1 g L^{-1}) prior to nanoprecipitation in the miscible non-solvent acetonitrile (1:7 v/v) as detailed in the experimental section. Thermal evaporation of all chloroform and some acetonitrile (70 °C) reduced the dispersion volume to 25%.

For small concentrations of iodine $\zeta_{I2/J71}$, we observed some coagulation of the polymer in dispersion that we attribute to an insufficient degree of doping. Thus, we sep-

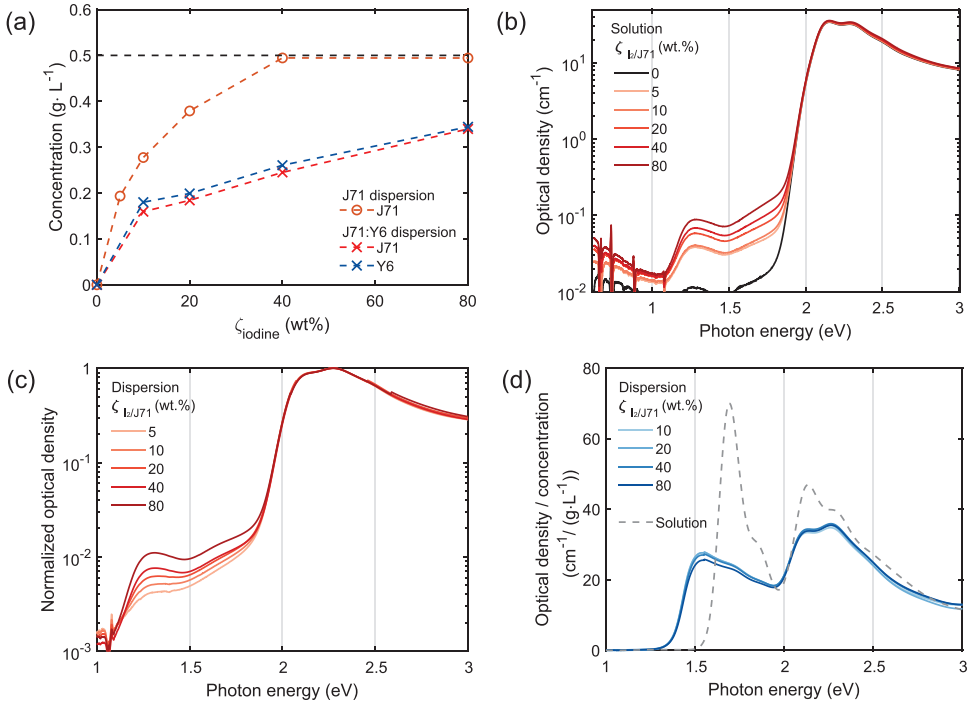

Figure 2. a) Concentration of the semiconductors J71 or J71:Y6 in dispersions (supernatant) versus the concentration of iodine $\zeta_{I2/J71}$ ($0 \leq \zeta_{I2/J71} \leq 80$ wt.%) after centrifugation. Dotted lines are drawn to guide the eye. b) The optical densities of J71 solutions after the addition of iodine show a relative increase of the polaron signature at 1.3 eV for higher doping ratios. c) Normalized optical densities of the corresponding iodine-stabilized J71 dispersions after nanoprecipitation into acetonitrile and thermal reduction. The polaron signatures persist. d) Optical densities of iodine-stabilized J71:Y6/acetonitrile dispersions ($10 \leq \zeta_{I2/J71} \leq 80$ wt.%) per J71 concentration and, for reference, a J71:Y6/chloroform solution (1 g L^{-1}).

arated stabilized nanoparticles from non-stabilized larger polymer agglomerates by centrifugation (14100 g; 2 min), removed the sediments and analyzed the supernatant. **Figure 2**a shows the semiconductor concentration in the supernatant, i.e., the concentration of electrostatically stabilized polymer nanoparticles, which was determined by redissolution of the dispersion and comparison of its absorption to solutions of known concentrations. Without any iodine, the dispersions coagulated within seconds, which led to the total removal of the organic semiconductor from the supernatant. For increasing $\zeta_{I2/J71}$, the nanoparticle concentration in the supernatant increased until, when exceeding $\zeta_{I2/J71}$ = 40 wt.%, almost all polymer remained in dispersion. With increasing $\zeta_{I2/J71}$, we also observed a reduction of the nanoparticle size (Table S1, Supporting Information) as more charges can stabilize larger surfaces and hence produce smaller nanoparticles.[5] Smaller amounts of iodine than $\zeta_{I2/J71}$ = 10 wt.% resulted in too large (nano)particles and too low dispersion concentrations that were useless to any of the later device experiments.

More detailed insights into the doping and stabilization mechanisms were gained from monitoring the charge transfer using UV-Vis-NIR spectrometry. Figure 2b,c compare the optical densities of the J71/iodine/chloroform solutions and the J71/iodine/acetonitrile dispersions on logarithmic scale at different iodine/J71 mass ratios $\zeta_{I2/J71}$. Since large agglomerates were removed from the dispersions by centrifugation and hence the concentrations of the dispersions varied with the amount of iodine, the optical densities of the dispersions were normalized to the J71 peak.

In both solution and dispersion, J71 absorbs above its optical gap of 2.1 eV exhibiting two vibronic peaks at 2.15 and 2.3 eV. Upon nanoprecipitation and hence nanoparticle formation, the relative magnitude of the two vibronic features changes for all $\zeta_{I2/J71}$. The peak at 2.15 eV is stronger in solution, whereas the peak at 2.3 eV prevails in dispersion. This effect has been reported in the earlier literature, upon the formation of J71 thin films.[17] We consider this change of relative peak heights an indicator that solid nanoparticles have formed during nanoprecipitation. We note that the spectral change from solution to dispersion is reversible upon re-dissolution of the nanoparticles in chloroform, which lets us exclude any effects from degradation of the polymer (Figure S1, Supporting Information).

While the addition of iodine hardly influences the characteristic main absorption, a new absorption feature emerges with a peak energy of 1.3 eV in both solution and dispersion. The formation of an electronic transition below the optical gap of a neutral p-type polymer is often attributed to the formation of polarons after charge transfer and hence electrical doping.[18,19,28–30,20–27] The evolution of two electronic transitions has been reported on other polymers, one just below the optical gap of the neutral polymer (P2) and the other with an even lower energy (P1).[31–38] Likewise, we attribute the peak at 1.3 eV of the absorption spectrum of J71 to P2, whereas P1 may be indicated by its onset below 1 eV. Notably, the optical density of P2 is more than two orders of magnitudes weaker than the main absorption, which we attribute to a rather moderate doping efficiency. This interpretation is in accordance

Table 1. Key parameters of the nanoparticulate J71:Y6 solar cells in dependence of the mass ratio $\zeta_{I2/J71}$. Below $\zeta_{I2/J71}$ = 20 wt.%, no stable nanoparticle dispersions could be produced.

$\zeta_{I2/J71}$ [wt.%]	Thickness [nm][a)]	Deposition steps[b)]	V_{OC} [mV]	J_{SC} [mA cm^{-2}]	J_{SC}* [mA cm^{-2}][c)]	FF [%]	PCE [%][d)]	N[e)]
20	80	50	706 ± 2	24.2 ± 0.2	23.3	60.4 ± 0.5	10.2 ± 0.1 (10.3)	8/8
40	85	30	712 ± 2	24.2 ± 0.2	23.1	60.8 ± 0.8	10.4 ± 0.2 (10.6)	12/12
60	85	25	709 ± 2	23.8 ± 0.3	23.0	61.1 ± 0.6	10.2 ± 0.1 (10.3)	14/16
80	90	23	709 ± 1	24.2 ± 0.2	23.5	59.4 ± 0.4	10.1 ± 0.1 (10.3)	16/16
120	85	23	692 ± 3	23.5 ± 0.2	22.7	60.6 ± 0.5	9.7 ± 0.2 (9.9)	8/8
0[f)]	70	1	791 ± 5	20.2 ± 0.1	20.0	57.0 ± 1.0	9.1 ± 0.2 (9.3)	4/4
0[g)]	90	1	806 ± 3	19.3 ± 0.2	19.8	37.2 ± 0.2	5.8 ± 0.1	8/8

[a)]Thickness of the nanoparticulate light-harvesting layer rounded to 5 nm; [b)]Number of sequential spin coating steps required to reach the specified layer thickness; [c)]Integrated current densities calculated by multiplying the EQE with AM 1.5G for one representative solar cell; [d)]PCE of hero devices in parentheses; [e)]Number of properly working samples versus number of fabricated samples; [f)]deposition from chlorobenzene solution for reference; [g)]deposition from chloroform solution for reference.

with an oxidation potential E_{ox} = 0.55 eV of J71 and a reduction potential E_{red} = –0.11 eV of iodine (both against ferrocene in acetonitrile).[39,40] Accordingly, the P2 peak gains strength for increasing $\zeta_{I2/J71}$, which indicates a gradually stronger positive charging of J71.

Next, we extended our efforts to J71:Y6 bulk-heterojunction nanoparticle dispersions which are needed to fabricate organic solar cells. Therefore, we prepared a blend solution of J71 and Y6 in chloroform (each 1 g L^{-1}) and conducted the nanoprecipitation as described above. As depicted in Figure 2a, the stabilization of the bulk-heterojunction nanoparticle dispersions was less efficient and larger amounts of iodine were needed. The reason for the reduced dispersion stability can be found in the role of Y6. Control experiments on neat Y6 have shown that even the highest concentration of iodine did not lead to the formation of nanoparticles, but instead, neat Y6 coagulated immediately. This finding appears reasonable, as the ionization potential of Y6 is too large to undergo p-doping by iodine. Thus, we conclude that only polarons on J71 account for the charging of J71:Y6 nanoparticles and hence the dispersion stability. Figure 2d compares the optical densities of a J71:Y6 solution with the optical densities of J71:Y6 dispersions of different iodine concentration. In order to allow a meaningful comparison, the optical densities were divided by the J71 concentration. The optical density of J71 shows the same evolution as in neat J71 dispersions. In addition, the main absorption peak of Y6 is red-shifted due to the excitonic coupling of aggregated molecules inside the nanoparticles, which was previously reported during layer deposition and solidification.[41,42] The ratio of J71 and Y6 is about the same in all dispersions which lets us conclude that Y6 is firmly incorporated into the nanoparticles during the rapid nanoparticle formation upon nanoprecipitation. The bulk-heterojunction is "frozen" in a non-equilibrium state inside the nanoparticles, preventing demixing.

Finally, we fabricated organic solar cells from the iodine-stabilized J71:Y6 nanoparticle dispersions. Therefore, we spin cast light-harvesting layers from the ready-to-use dispersions and incorporated them into a regular device architecture comprising glass/ITO/PEDOT:PSS/J71:Y6/ZnO/Ag. As common for most light-harvesting layers that are spin cast from nanoparticle dispersions, multiple deposition steps were needed to achieve sufficient layer thicknesses (**Table 1**). The higher the iodine to J71 mass ratio $\zeta_{I2/J71}$, the larger is the amount of J71:Y6 that can be held in dispersion, and the smaller is the number of repetitive coating steps. Notably, the number of deposition steps could be further reduced by employing doctor blading or inkjet printing, but this goes beyond the scope of this paper.[43] After deposition, the nanoparticulate layers were thermally annealed (180 °C, 10 min) to merge the nanoparticles for better transport of photogenerated charge carriers (see also atomic force micrographs in Figure S3, Supporting Information). This merging of nanoparticles upon thermal annealing in the light-harvesting layers promotes the formation of closed layers and hence renders the nanoparticle size of less a concern. In addition, the atomic force tapping phase images in Figure S3d–f (Supporting Information) suggest a homogenization of the film composition during thermal annealing, improving average domain sizes and hence photocurrent generation. At the same time, thermal annealing efficiently drives the iodine out of the organic thin film.[44] Therefore, we expect only negligible effects of residual iodine on the solar cell performance if any. Energy-dispersive X-ray analysis did not show any traces of iodine left in the thin-film (i.e., the remaining iodine must be less than 0.3 wt.%, data not shown here). The current density – voltage (J–V) curves of representative solar cells are depicted in **Figure 3**a and the corresponding key parameters of the solar cells, i.e., open-circuit voltage (V_{OC}), short-circuit current (J_{SC}), fill factor (FF), and PCE, are summarized in Table 1.

The external quantum efficiencies (EQEs) which are depicted in Figure 3b, attest a broad contribution to the photocurrent across the absorption of J71 and Y6 (430-860 nm).

All solar cells produce a remarkable J_{sc} on the order of 24 mA cm^{-2}, which is well in agreement with the J_{sc}^{*} calculated from the integrated external quantum efficiencies (EQEs) of the devices in Figure 3b. Together with a FF of about 61%, most solar cells yielded a PCE in excess of 10%. The highest PCE of 10.4% (hero device: 10.6%) was achieved at $\zeta_{I2/J71}$ = 40 wt.% and with an annealing temperature of 180 °C. A fill factor above 60% is impressive for organic solar cells

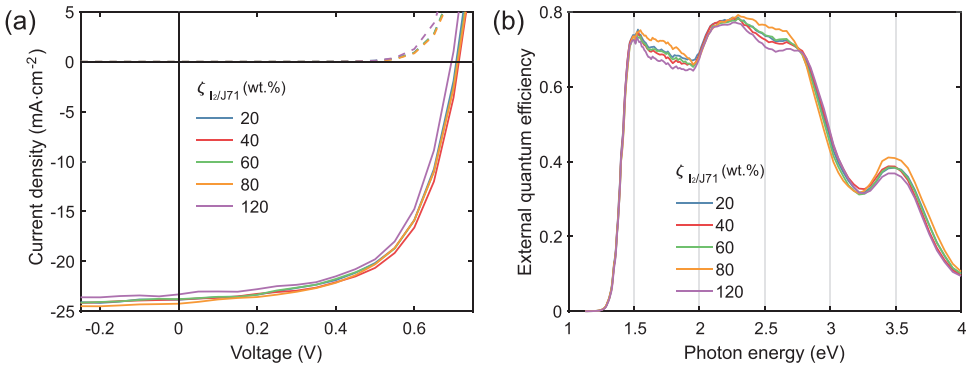

Figure 3. a) *J–V* curves of representative nanoparticulate J71:Y6 solar cells at different iodine to J71 mass ratios $\zeta_{I2/J71}$ under 1 sun irradiation (solid lines) and in the dark (dashed lines). b) Corresponding EQE measurements of the solar cells.

fabricated from nanoparticle dispersion, where only thermal annealing and no solvent additives were used to tailor the microstructure. Even though the light-harvesting layers were fabricated from nanoparticle dispersions which are commonly perceived to be prone to shunting, we obtained an excellent total yield of 62 out of 64 properly working solar cells. All solar cells fabricated from nanoparticle dispersions synthesized with iodine concentrations $\zeta_{I2/J71}$ between 20 wt.% and 80 wt.% achieved almost equally good performance, which marks a broad process window for the iodine doping. And even after 14 months of shelf-storage in a glovebox under nitrogen atmosphere, the performance of all solar cells remained within the specifications in Table 1. Very minor deterioration was observed in the FF only.

Remarkably, the efficiency of the nanoparticulate J71:Y6 solar cells even surpasses the performance of their counterparts processed from chloroform (5.8%) or chlorobenzene (9.3%). Solution processed J71:Y6 solar cells were reported to suffer from an unfavorable phase separation during the drying of the thin films, which led to FFs of 55%.[45,46] Only by using a chemically modified Y6 for less demixing, an efficiency of 11.6% was achieved.[47,48] Here, the "freezing" of the J71:Y6 bulk-heterojunction in an non-equilibrium state during the very fast nanoparticle formation within 100 ms[49] may well account for the improved performance of the solar cells.

3. Conclusion

By introducing reversible electrostatic stabilization (RES), we temporarily p-doped the polymer J71 in solution using iodine. This charging of the polymer promoted the electrostatic colloidal stabilization of J71 and J71:Y6 dispersions upon nanoprecipitation. Y6 was held in place inside the nanoparticles by J71. After J71:Y6 thin-film deposition from nanoparticle dispersion, thermal annealing of the bulk-heterojunction led to the evaporation of iodine, and the corresponding solar cells produced PCEs of up to 10.6%. Thus, our experiments clearly demonstrated that solar cells that were deposited from dispersions of high-performance semiconductors, can yield high performances that are competitive to devices processed along common solution deposition routes.

Notably, the amount of iodine of 40 wt.% needed for p-doping is comparably large which can be attributed to the weak doping from iodine. Future efforts may investigate stronger and more efficient dopants to replace iodine. However, the charge transfer between a stronger dopant and the polymer will not be as easily reversible, and therefore the dopant will likely exhibit less volatility after thin film deposition. It will be this trade-off of doping strength and volatility that will guide future explorations on how to best stabilize organic nanoparticle dispersions in absence of prevailing surfactants. Therefore, doping with iodine is not a universal concept by itself to electrostatically stabilize organic nanoparticle dispersions. Electrostatic stabilization requires an efficient charge transfer between the polymer and the dopant, and thus a harmonized energy landscape of the two components.

4. Experimental Section

Materials: Y6 (BTP-4F) was purchased from 1-material; J71 from Ossila. All organic semiconductors were used as received without further purification and stored under nitrogen atmosphere. Spherical solid iodine was stored under nitrogen atmosphere. Acetonitrile (anhydrous, 99.8%), and chloroform (analytical grade) were purchased from Merck and used without further purification.

Preparation of Semiconductor Solutions: J71 and Y6 were dissolved separately in chloroform (4 g L^{-1}, 45 °C) for at least 20 min and mixed in equal volumes. Iodine was dissolved in chloroform (10 g L^{-1}) at least 1 h before use. The semiconductor solutions were doped by adding the respective volume of iodine solution to the semiconductor solution and then diluted to yield the same concentration for all doping ratios (J71: 1 g L^{-1}; Y6: 1 g L^{-1}).

Nanoparticle Synthesis: Organic nanoparticle dispersions were synthesized by nanoprecipitation. One milliliter of the doped semiconductor solutions were injected into 7 mL of acetonitrile within 0.8 s under vigorous stirring. The immediate reduction of solubility led to the rapid formation of organic semiconductor nanoparticles. Then the dispersions were heated at 70 °C, until the chloroform was removed and the concentration of the dispersion had increased to 1 g L^{-1}. Afterwards, agglomerates were removed by centrifugation (Eppendorf MiniSpin plus, 14 500 rpm; 14 100 g, 2 min). The amount of sediment strongly depended on the iodine concentration.

Measurement of the Dispersion Concentration: The acetonitrile dispersion was diluted with chloroform (1:40 v/v) to fully dissolve the nanoparticles. The concentration was determined by deconvolution of the optical density of the solute into contributions from J71 and Y6 using a least-square fit and comparison with reference solutions.

Deposition of J71:Y6 Layers: The J71:Y6 layers were iteratively spin cast from dispersion (800 rpm, 23–50 times). The number of casting steps was adjusted to reach the same layer thickness of 90 nm. The deposition was stopped, when the perceived optical density of the light-harvesting layer equaled a reference layer with the desired layer thickness. Afterwards, the sample was thermally annealed on a hotplate (180°C, 10 min).

Fabrication of J71:Y6 Organic Solar Cells: Solar cells were fabricated with regular device architecture. Indium tin oxide (ITO) covered glass substrates were cleaned by wiping with cleanroom tissue and isopropanol, and by ultrasonication in acetone (10 min). Remaining visible particles were removed by a polyester swab and detergent. Afterwards, the substrates were ultrasonicated in isopropanol (10 min) and treated with an oxygen plasma (2 min). PEDOT:PSS (CLEVIOS™ P VP AI 4083, Heraeus) was filtered (pore size 0.45 µm) and spin cast (5000 rpm, 30 s) to form the hole transport layer (30 nm). Then the samples were thermally annealed on a hotplate (150 °C, 10 min) under ambient conditions. All subsequent process steps were carried out under inert conditions (<10 ppm oxygen, <10 ppm water). The J71:Y6 light-harvesting layers from nanoparticle dispersion were deposited as described above. For reference, solar cells were fabricated from solution. Therefore, J71 and Y6 were dissolved separately in chlorobenzene (26 g L^{-1}) or chloroform (20 g L^{-1}) and mixed 1:1 by volume. The solution was spin cast (chlorobenzene: 1400 rpm, 30 s, 50 µL; chloroform: 3000 rpm, 20 s, 50 µL) without subsequent thermal annealing. On top, an electron transport layer (10 nm) was spin cast (2000 rpm, 40 s) from zinc oxide nanoparticles, synthesized as described in the literature, and dried on a hotplate (80 °C, 10 min).[50] The silver top electrode (100 nm) was sublimed in high vacuum (base pressure ≤ 1· 10^{-6} mbar).

Solar Cell Characterization: The solar cells were measured under standard conditions (1 sun, AM 1.5G) in nitrogen atmosphere. A high power xenon solar simulator (Sciencetech, Lightline AX-LA200, Classification AAA, ASTM E927) was used to generate AM 1.5G illumination, and its output power was adjusted by a silicon reference solar cell with a KG5 filter (Newport 91150-KG5) to match 1 sun. A current-voltage sweep from –1.5 V to 1.5 V with 50 mV step size was performed by a source meter unit (Keithley 2420) in 4-wire mode. The spectral mismatch factor was determined according to ASTM E973 (without tracking the temperature) by measuring the EQE of each solar cell variation and used to calculate corrected currents.

External Quantum Efficiency (EQE): A home-build setup was used to measure the wavelength-dependent EQE. Broadband white light was generated by a xenon high-pressure lamp (450 W, LSH601, LOT Oriel) and guided into a Cerny-Turner-monochromator (Omni-λ300, LOT Oriel with a MSZ3122, LOT Oriel filter wheel) that allowed the sequential selection of monochromatic light. The monochromatic light was optically chopped (C-995, Terahertz Technologies) with 373 Hz. The output light was split into two beams. The first beam was focused on a monitor photodiode (K1713-09, Hamamatsu) to track fluctuations of the xenon high-pressure lamp. The second beam was coupled into an optical fiber (fiber patch cable M37L02, Thorlabs). The fiber guided the light into an inert nitrogen glovebox. The light was decoupled and focused onto the measurement sample with a diameter of 1 mm. The currents of the sample and of the monitor diode were converted into an amplified voltage by two transimpedance amplifiers (OE-200S, Femto Messtechnik). The resulting voltage signal was measured by a lock-in amplifier (eLockIn 203, Anfatec Instruments) with a settling time and an integration time of 2 s each. The setup was referenced to a calibrated photodiode (818-UV-20925, Newport Corporation, calibrated per procedure no PTP99163 by Newport Corporation in December 2020 with traceability no O-0000000544) to obtain the spectral response.

Supporting Information

Supporting Information is available from the Wiley Online Library or from the author.

Acknowledgements

This work was financed by the German Ministry of Education and Research (BMBF) under contract no. 03EK3571 (project TAURUS II) and later by the Helmholtz research program "Materials and Technologies for the Energy Transition (MTET)." K.F. received funding from the Graduate School for Climate and Environment (GRACE). The authors thank Alexander D. Schulz for AFM measurements and David J. Jones (The University of Melbourne) for fruitful discussions.

Open access funding enabled and organized by Projekt DEAL.

Conflict of Interest

The authors declare no conflict of interest.

Data Availability Statement

The data that support the findings of this study are available from the corresponding author upon reasonable request.

Keywords

electrical doping, nanoparticles, nanoprecipitation, non-fullerene acceptors, organic solar cells

Received: August 17, 2022
Revised: November 6, 2022
Published online:

[1] N. E. Jackson, K. L. Kohlstedt, B. M. Savoie, M. Olvera de la Cruz, G. C. Schatz, L. X. Chen, M. A. Ratner, *J. Am. Chem. Soc.* **2015**, *137*, 6254.
[2] Y. Cui, H. Yao, L. Hong, T. Zhang, Y. Xu, K. Xian, B. Gao, J. Qin, J. Zhang, Z. Wei, J. Hou, *Adv. Mater.* **2019**, *14*, 1808356.
[3] L. Hong, H. Yao, Z. Wu, Y. Cui, T. Zhang, Y. Xu, R. Yu, Q. Liao, B. Gao, K. Xian, H. Y. Woo, Z. Ge, J. Hou, *Adv. Mater.* **2019**, *31*, 1903441.
[4] S. Gärtner, M. Christmann, S. Sankaran, H. Röhm, E.-M. Prinz, F. Penth, A. Pütz, A. E. Türeli, B. Penth, B. Baumstümmler, A. Colsmann, *Adv. Mater.* **2014**, *26*, 6653.
[5] F. Manger, P. Marlow, K. Fischer, M. Nöller, C. Sprau, A. Colsmann, *Adv. Funct. Mater.* **2022**, *32*, 2202566.
[6] S. Gärtner, S. Reich, M. Bruns, J. Czolk, A. Colsmann, *Nanoscale* **2016**, *8*, 6721.
[7] P. Marlow, F. Manger, K. Fischer, C. Sprau, A. Colsmann, *Nanoscale* **2022**, *14*, 5569.
[8] C. Xie, T. Heumüller, W. Gruber, X. Tang, A. Classen, I. Schuldes, M. Bidwell, A. Späth, R. H. Fink, T. Unruh, I. McCulloch, N. Li, C. J. Brabec, *Nat. Commun.* **2018**, *9*, 5335.
[9] H. Takeuchi, M. Kobashi, *Chem. Lett.* **1999**, *28*, 415.
[10] H. Shimizu, M. Yamada, R. Wada, M. Okabe, *Polym J* **2008**, *40*, 33.
[11] C. Xie, X. Tang, M. Berlinghof, S. Langner, S. Chen, A. Späth, N. Li, R. H. Fink, T. Unruh, C. J. Brabec, *ACS Appl. Mater. Interfaces* **2018**, *10*, 23225.
[12] C. Xie, A. Classen, A. Späth, X. Tang, J. Min, M. Meyer, C. Zhang, N. Li, A. Osvet, R. H. Fink, C. J. Brabec, *Adv. Energy Mater.* **2018**, *8*, 1702857.
[13] L. D'Olieslaeger, G. Pirotte, I. Cardinaletti, J. D'Haen, J. Manca, D. Vanderzande, W. Maes, A. Ethirajan, *Org. Electron.* **2017**, *42*, 42.
[14] P. C. Van Der Hoeven, J. Lyklema, *Adv. Colloid Interface Sci.* **1992**, *42*, 205.

[15] J. H. Burke, M. J. Bird, *Adv. Mater.* **2019**, *31*, 1806863.
[16] C. K. Chiang, M. A. Druy, S. C. Gau, A. J. Heeger, E. J. Louis, A. G. MacDiarmid, Y. W. Park, H. Shirakawa, *J. Am. Chem. Soc.* **1978**, *100*, 1013.
[17] H. Bin, Y. Yang, Z. Peng, L. Ye, J. Yao, L. Zhong, C. Sun, L. Gao, H. Huang, X. Li, B. Qiu, L. Xue, Z. Zhang, H. Ade, Y. Li, *Adv. Energy Mater.* **2018**, *8*, 1702324.
[18] R. Österbacka, C. P. An, X. M. Jiang, Z. V. Vardeny, *Science* **2000**, *287*, 839.
[19] C. Wang, D. T. Duong, K. Vandewal, J. Rivnay, A. Salleo, *Phys. Rev. B* **2015**, *91*, 085205.
[20] P. Pingel, D. Neher, *Phys. Rev. B* **2013**, *87*, 115209.
[21] H. Méndez, G. Heimel, S. Winkler, J. Frisch, A. Opitz, K. Sauer, B. Wegner, M. Oehzelt, C. Röthel, S. Duhm, D. Többens, N. Koch, I. Salzmann, *Nat. Commun.* **2015**, *6*, 8560.
[22] P. Pingel, M. Arvind, L. Kölln, R. Steyrleuthner, F. Kraffert, J. Behrends, S. Janietz, D. Neher, *Adv. Electron. Mater.* **2016**, *2*, 1600204.
[23] M. Arvind, C. E. Tait, M. Guerrini, J. Krumland, A. M. Valencia, C. Cocchi, A. E. Mansour, N. Koch, S. Barlow, S. R. Marder, J. Behrends, D. Neher, *J. Phys. Chem. B* **2020**, *124*, 7694.
[24] D. T. Scholes, P. Y. Yee, J. R. Lindemuth, H. Kang, J. Onorato, R. Ghosh, C. K. Luscombe, F. C. Spano, S. H. Tolbert, B. J. Schwartz, *Adv. Funct. Mater.* **2017**, *27*, 1702654.
[25] J. Yamamoto, Y. Furukawa, *J. Phys. Chem. B* **2015**, *119*, 4788.
[26] R. Ghosh, A. R. Chew, J. Onorato, V. Pakhnyuk, C. K. Luscombe, A. Salleo, F. C. Spano, *J. Phys. Chem. C* **2018**, *122*, 18048.
[27] N. M. B. Neto, M. D. R. Silva, P. T. Araujo, R. N. Sampaio, *Adv. Mater.* **2018**, *30*, 1705052.
[28] Y. Yamashita, J. Tsurumi, M. Ohno, R. Fujimoto, S. Kumagai, T. Kurosawa, T. Okamoto, J. Takeya, S. Watanabe, *Nature* **2019**, *572*, 634.
[29] Y. Liu, B. Nell, K. Ortstein, Z. Wu, Y. Karpov, T. Beryozkina, S. Lenk, A. Kiriy, K. Leo, S. Reineke, *ACS Appl. Mater. Interfaces* **2019**, *11*, 11660.
[30] Y. Karpov, T. Erdmann, I. Raguzin, M. Al-Hussein, M. Binner, U. Lappan, M. Stamm, K. L. Gerasimov, T. Beryozkina, V. Bakulev, D. V. Anokhin, D. A. Ivanov, F. Günther, S. Gemming, G. Seifert, B. Voit, R. Di Pietro, A. Kiriy, *Adv. Mater.* **2016**, *28*, 6003.
[31] C. Enengl, S. Enengl, S. Pluczyk, M. Havlicek, M. Lapkowski, H. Neugebauer, E. Ehrenfreund, *ChemPhysChem* **2016**, *17*, 3836.
[32] M. G. Voss, J. Reddy Challa, D. Tyler Scholes, P. Y. Yee, E. C. Wu, X. Liu, S. J. Park, O. León Ruiz, S. Subramaniyan, M. D. Chen, S. A. Jenekhe, X. L. Wang, S. H. Tolbert, B. J. Schwartz, M. G. Voss, J. R. Challa, D. T. Scholes, P. Y. Yee, E. C. Wu, X. Liu, S. J. Park, O. León Ruiz, X. L. Wang, S. H. Tolbert, B. J. Schwartz, S. Subramaniyan, S. A. Jenekhe, M. D. Chen, O. L. Ruiz, S. Subramaniyan, et al., *Adv. Mater.* **2021**, *33*, 2000228.
[33] G. Heimel, *ACS Cent. Sci.* **2016**, *2*, 309.
[34] I. Salzmann, G. Heimel, M. Oehzelt, S. Winkler, N. Koch, *Acc. Chem. Res.* **2016**, *49*, 370.
[35] I. E. Jacobs, A. J. Moulé, *Adv. Mater.* **2017**, *29*, 1703063.
[36] T. J. Aubry, K. J. Winchell, C. Z. Salamat, V. M. Basile, J. R. Lindemuth, J. M. Stauber, J. C. Axtell, R. M. Kubena, M. D. Phan, M. J. Bird, A. M. Spokoyny, S. H. Tolbert, B. J. Schwartz, *Adv. Funct. Mater.* **2020**, *30*, 2001800.
[37] I. Zozoulenko, A. Singh, S. K. Singh, V. Gueskine, X. Crispin, M. Berggren, *ACS Appl Polym Mater* **2019**, *1*, 83.
[38] M. G. Voss, D. T. Scholes, J. R. Challa, B. J. Schwartz, *Faraday Discuss.* **2019**, *216*, 339.
[39] C. L. Bentley, A. M. Bond, A. F. Hollenkamp, P. J. Mahon, J. Zhang, *J. Phys. Chem. C* **2015**, *119*, 22392.
[40] Y. Li, L. Zhong, B. Gautam, H.-J. Bin, J.-D. Lin, F.-P. Wu, Z. Zhang, Z.-Q. Jiang, Z.- G. Zhang, K. Gundogdu, Y. Li, L.-S. Liao, *Energy Environ. Sci.* **2017**, *10*, 1610.
[41] D. Li, X. Zhang, D. Liu, T. Wang, *J. Mater. Chem. A* **2020**, *8*, 15607.
[42] L. Zhu, M. Zhang, G. Zhou, T. Hao, J. Xu, J. Wang, C. Qiu, N. Prine, J. Ali, W. Feng, X. Gu, Z. Ma, Z. Tang, H. Zhu, L. Ying, Y. Zhang, F. Liu, *Adv. Energy Mater.* **2020**, *10*, 1904234.
[43] S. Sankaran, K. Glaser, S. Gärtner, T. Rödlmeier, K. Sudau, G. Hernandez-Sosa, A. Colsmann, *Org. Electron.* **2016**, *28*, 118.
[44] I. E. Jacobs, J. Li, S. L. Burg, D. J. Bilsky, B. T. Rotondo, M. P. Augustine, P. Stroeve, A. J. Moulé, *ACS Nano* **2015**, *9*, 1905.
[45] G. Xie, Z. Zhang, Z. Su, X. Zhang, J. Zhang, *Nano Energy* **2020**, *69*, 104447.
[46] X. Ma, Q. An, O. A. Ibraikulov, P. Lévêque, T. Heiser, N. Leclerc, X. Zhang, F. Zhang, *J. Mater. Chem. A* **2020**, *8*, 1265.
[47] C. Xu, J. Wang, Z. Zhao, J. Gao, Z. Hu, X. Ma, X. Zhang, F. Zhang, *Sustain. Energy Fuels* **2020**, *4*, 3979.
[48] Y. Wang, C. Xu, C. Wang, Y. Yan, Q. Sun, X. Ma, F. Zhang, *J. Polym. Sci.* **2022**, *60*, 968.
[49] K. Fischer, P. Marlow, F. Manger, C. Sprau, A. Colsmann, *Adv. Mater. Technol.* **2022**, 2200297.
[50] B. Sun, H. Sirringhaus, *Nano Lett.* **2005**, *5*, 2408.